Journal of Trace Elements in Medicine and Biology 51 (2019) 191–203

Contents lists available at ScienceDirect

Journal of Trace Elements in Medicine and Biology

journal homepage: www.elsevier.com/locate/jtemb

Toxicology

Crustin-capped selenium nanowires against microbial pathogens and Japanese encephalitis mosquito vectors – Insights on their toxicity and internalization

Ravichandran Rekha[a], Baskaralingam Vaseeharan[a,*], Sekar Vijayakumar[a], Muthukumar Abinaya[a], Marimuthu Govindarajan[b,c], Naiyf S. Alharbi[d], Shine Kadaikunnan[d], Jamal M. Khaled[d], Mohammed N. Al-anbr[d]

[a] Biomaterials and Biotechnology in Animal Health Lab, Department of Animal Health and Management, Alagappa University, Karaikudi, 630 004, Tamil Nadu, India
[b] Unit of Vector Control, Phytochemistry and Nanotechnology, Department of Zoology, Annamalai University, Annamalainagar, 608 002, Tamil Nadu, India
[c] Department of Zoology, Government College for Women, Kumbakonam, 612 001, Tamil Nadu, India
[d] Department of Botany and Microbiology, College of Science, King Saud University, Riyadh, 11451, Saudi Arabia

ARTICLE INFO

Keywords:
Biocompatibility
Culex quinquefasciatus
Culex tritaeniorhynchus
Integrated vector management
Mosquito control
Culicidae
Nanomaterial
Pesticide

ABSTRACT

Herein, we reported a method to synthesize selenium nanowires (Cr-SeNWs) relying to purified cysteine-rich antimicrobial peptide crustin in presence of ascorbic acid. Cr-SeNWs were characterized by UV–vis, XRD, FTIR and Raman spectroscopy, as well as SEM, HR-TEM and EDAX. The UV–vis spectroscopy peak was noted at 350 nm. XRD showed the crystalline nature of Cr-SeNWs through diffraction peaks observed 2θ at 12° and 28° corresponding to (020), and (241) lattice planes, respectively. HR-TEM results shed light on the size of Cr-SeNWs, ranging from 17 to 47 nm. Raman spectroscopy and EDAX analysis of Cr-SeNWs showed presence of 57% selenium element. Furthermore, Cr-SeNWs showed higher antimicrobial activity on Gram-positive bacteria (*Staphylococcus aureus*, *Enterococcus faecalis)* over Gram-negative ones (*Pseudomonas aeruginosa*, *Escherichia coli)*. The zone of inhibition was larger on *S. aureus* (50 μg/ml = 4.0 mm, 75 μg/ml = 7.2 mm) and *E. faecalis* (50 μg/ml = 3.1 mm, 75 μg/ml = 5.1 mm), over *P. aeruginosa* (50 μg/ml = 2.1 mm, 75 μg/ml = 4.8 mm), *E. coli* (50 μg/ml = 1.3 mm, 75 μg/ml = 4.3 mm) bacteria. The antibiofilm activity of Cr-SeNWs was also investigated and biofilm reduction was observed at 75 μg/ml. In addition, Cr-SeNWs were highly effective as larvicides against Zika virus and Japanese encephalitis mosquito vectors, i.e., *Culex quinquefasciatus* and *Culex tritaeniorhynchus*, with LC_{50} values of 4.15 and 4.85 mg/l, respectively. The nanowire toxicity and internalization was investigated through confocal laser scanning microscopy and histological studies. To investigate the potential of Cr-SeNWs for real-world applications, we also evaluated Cr-SeNWs in hemolytic assays, showing no cytotoxicity till 5 mg/ml. Besides, higher antioxidant activity at the concentration at 100 μg/ml was noted, if compared with purified crustin. The strong antioxidant potential of this nanomaterial can be helpful to boost the shelf-life potential of Cr-SeNWs-based pesticides and antimicrobials.

1. Introduction

Managing mosquito vectors and microbial pathogens is a challenge for current research in public health and entomology [1], worsened by the quick drug and pesticide resistance development in targeted species [2]. A number of species belonging to the genera *Anopheles, Aedes* and *Culex* still act as major vectors of mosquito-borne diseases affecting and killing millions of humans and other animals per year in tropical and sub-tropical regions [3,4]. In particular, arboviral threats are rapidly growing in the latest decade, with the raise of dengue, West Nile, chikungunya and Zika virus cases over time [5,6]. Several *Culex* species can act as vectors of Japanese encephalitis, Zika virus, St. Louis encephalitis virus, and Western equine encephalitis virus [7] globally, up to 20,400 human deaths are caused by Japanese encephalitis, with more than 50,000 clinical cases in each year. Primarily, it affects children and no antiviral treatment is currently available for infected patients [8].

The frequent overuse of commercial pesticides for vector control operations leads to the resistance development and is also detrimental to human health and the environment [9], therefore researchers are

* Corresponding author.
E-mail address: vaseeharanb@gmail.com (B. Vaseeharan).

https://doi.org/10.1016/j.jtemb.2018.10.017
Received 26 July 2018; Received in revised form 12 October 2018; Accepted 16 October 2018

looking to novel and more eco-friendly tools to manage vector populations and parasites [10–21].

A similar scenario applies well to microbial pathogens. Microbial cells in various ecosystems frequently live in surface-attached and densely clustered communities, i.e., biofilms, to defend themselves from hard environmental conditions [22]. Biofilms play a fundamental role in healthcare-associated severe infections. Biofilm-related bacteria provide vast tolerance towards host immune defense mechanisms and antibiotics often ensuing in persistent and hard to treat infections [23]. Hence, alternative drugs are urgently needed to fight biofilm-forming pathogens of clinical relevance [24].

Nanobiotechnology currently plays a key role in diagnostics, pharmacology, chemical industries, environmental research, engineering, electronics and entomology [25,26]. Biomolecules such as proteins and carbohydrates as well as secondary metabolites of plant and animals can be used for the successful fabrication of nanomaterials with wide biomedical applications [27–29]. Among biomolecules with a role in the invertebrate immune system, antimicrobial peptides – such as crustin and penaeidin – are useful for bacterial control, as well as to inhibit the growth of bacterial pathogens [30], including biofilm-forming ones [31]. Crustin is a cationic cysteine rich 7–14 KDa antimicrobial peptide, widely found in marine especially in crustacean haemolymph. It contains various domains, including glycine, proline-rich and whey acidic protein in N and C terminus regions, respectively [32].

Selenium is a trace element naturally found in various biological sources, it represents an essential supplement in living organisms [33]. Yeast enriched with selenium can be used for supplementation and as well as for enrichment of various organisms by administration of sodium selenite [34,35]. Selenium-based synthesis of nanostructures has been shown as a useful biomedical tool, with special reference to anticancer activity [36,37], cancer prevention through molecular mechanisms [38], antioxidant properties [39], antidiabetic potential [40]. On the other hand, in vitro toxicity studies with mice model have been also done [41]. Notably, it has been never used for the synthesis of nanoproducts helpful to fight insect vectors and pathogenic bacteria. Earlier reports on the synthesis of selenium nanostructures relied to the employ of polysaccharides [42] and proteins (e.g., keratin, bovine serum albumin) [43], for various biomedical purposes. In another study, selenium nanowires have been synthesized using cytochrome C [44] and β-carotene [45].

Generally, the synthesis of nanoparticles using different chemical and physical routes is used. Widely adopted procedures includes heat evaporation, photochemical and electrochemical reduction, however these methods are expensive, time consuming and environmentally toxic [46]. Nowadays, focusing on alternative, eco-friendly synthesis protocols to fabricate nano materials using “green” reducing and stabilizing compounds from natural products research (e.g., proteins, plant extracts and biopolymers) is a fast-growing field of research interest [47,48]. However, little has been done to fabricate selenium nanostructures with eco-friendly molecules isolated from invertebrates, studying them against mosquito vectors and biofilm-forming bacteria.

Herein, selenium nanowires (Cr-SeNWs) were synthesized using purified cysteine-rich antimicrobial peptide crustin in presence of ascorbic acid. Cr-SeNWs were characterized by UV–vis, XRD, FTIR and Raman spectroscopy, as well as SEM, HR-TEM and EDAX. Cr-SeNWs were tested for their antimicrobial activity on Gram-positive bacteria (*Staphylococcus aureus, Enterococcus faecalis)* and Gram-negative ones (*Pseudomonas aeruginosa, Escherichia coli)*. The antibiofilm activity of Cr-SeNWs was also investigated. Furthermore, they were evaluated as larvicides against Zika virus and Japanese encephalitis mosquito vectors, i.e., *Culex quinquefasciatus* and *Culex tritaeniorhynchus*. The nanowire mode of action was investigated through confocal laser scanning microscopy (CLSM) and histological studies. To study the potential of this nanomaterial for real-world applications, we evaluated Cr-SeNWs in hemolytic assays on red blood cells (RBCs), as well as their antioxidant activity, since the latter can be helpful to boost the shelf-life potential of Cr-SeNWs-based insecticides and antimicrobials.

2. Materials and methods

2.1. Chemicals and bacteria

Sodium selenite (NaS_2O_3), ascorbic acid ($C_6H_8O_6$), ethanol (C_2H_5OH), methanol (CH_3OH), acridine orange (235474), resazurin ($C_{12}H_7NO_4$) and crystal violet (c3886) were purchased from Sigma-Aldrich. We also used Live/Dead BacLight Bacterial Viability Kit (L7012-Molecular Probes, Invitrogen, Grand Island, NY, USA) and 2, 2-diphenyl-1-picrylhydrazyl hydrate (DPPH) (St. Louis, MO, USA). Nutrient broth (NB) and Luria Bertani agar (LBA) were purchased from HiMedia (India). The bacteria *Staphylococcus aureus* (MTCC 9542), *Enterococcus faecalis* (HQ 693279.1), *Pseudomonas aeruginosa* (HQ 4006631) and *Escherichia coli* (ATCC 25922) were used.

2.2. Crab haemolymph extraction and purification of crustin

P. pelagicus crabs were obtained from the coastal area of Mandapam, Ramanathapuram district, (9.2770 °N, 79.1252 °E) Tamil Nadu, India. They were rinsed with clean water to eliminate particles and then haemolymph was extracted in presence of anticoagulant solution. The haemolymph was centrifuged at 4000 × *g* for 10 min, the supernatant was collected and stored at −80 °C. The cell pellet was washed in 200 ml of 1× Tris buffer and the material was applied to a Blue-Sepharose column (8 × 1 cm). The column was rinsed with 1x Tris buffer at 3 ml min^{-1} and the crustin pellet was collected as the maximum density 1.2 ml fraction [31].

2.3. Synthesis of Cr-SeNWs

The synthesis of Cr-SeNWs followed by the method of Li et al. [49], with slight changes. Synthesis of Cr-SeNWs through sodium selenite and crustin as capping agent under the assistance of ascorbic acid was done at 37 °C. To fabricate Cr-SeNWs, 2 ml of crustin was mixed in sodium selenite solution (30 mM, 0.1 g per 100 ml) and the initiator ascorbic acid was added drop wise until the color changed to orange, highlighting the reduction reaction. After mixing, the solution was kept under vigorous magnetic stirring till we obtained fire red color solution, which indicates conversion of sodium selenite into selenium. The red solution was sealed and kept in the darkness for a week then centrifuged at 8000 × *g* for 10 min. The collected pellet was washed with water followed by deep freeze-drying at −80 °C and vacuum drying overnight. Cr-SeNWs as powder was stored at room temperature (37 °C) for further experiments.

2.4. Characterization of Cr-SeNWs

The characterization of Cr-SeNWs was performed through UV–vis spectroscopy at wavelengths ranging between 200–700 nm (UV-1800, Shimadzu, Japan), crystalline nature of Cr-SeNWs was analyzed by XRD (X'PERT PROPAN analytical, PHILIPS,USA). Capping molecules of Cr-SeNWs were studied by FTIR spectroscopy (Shimadzu, Japan). Morphology, size and shape of Cr-SeNWs were determined through SEM (SEM, JSM 6701F-6701, JPEG, India), HR-TEM (JOEL model instrument 1200 EX instrument, Japan), while phase structure and crystallinity was studied by SAED. Furthermore, Raman spectroscopy on Cr-SeNWs was do neat room temperature through Micro-Laser Raman (Seiki, Japan). The powder sample was analyzed with semiconductor laser source ($\lambda = 532$ nm) at a power of 50 mW and the resolution of the Raman spectrum was 1 cm^{-1} in the measured frequency region.

2.5. Antibacterial activity of Cr-SeNWs

The antibacterial activity of Cr-SeNWs was evaluated on the growth of Gram-positive *S. aureus*, *E. faecalis* and Gram-negative *P. aeruginosa, E. coli* bacteria. The antibacterial activity of Cr-SeNWs was tested by agar well diffusion method as described by Vijayakumar et al. [50]. The targeted organisms (10 µl or 0.1%) were inoculated in LB broth (pH 7.4) for 18 h and allow growing further subculture. LB agar plates were prepared into the sterile petriplate with 20 ml of molten media. Then the targeted isolates (0.1%) were spread on LB agar plates using sterilized cotton swabs. Solidified agar plane was bored with gel borer to make wells (7 mm diameter). The addition of Cr-SeNWs was done testing various concentrations, i.e., 50 µg ml^{-1} and 75 µg ml^{-1} in sterilized double distilled water (which acted as negative control) into separate wells. The plates were incubated at 37 °C for 24 h and triplicates were carried out for all tested species. After the formation of zones around the well measured with transparent glass ruler in mm. Antibacterial efficacy of Cr-SeNWs was compared with negative control.

2.5.1. Microtiter plate assay for MIC with resazurin dye

For determining the MIC value of Cr-SeNWs on different bacteria, we relied to the method by Thirunarayanan et al. [51]. In polystyrene ninety-six well plate, 50 µl nutrient broth were added to every well, along with 10 µl of 10^6 cfu/ml bacterial suspensions (OD_{600} = 1.2). Cr-SeNWs was added to each well at various concentrations (10–100 µg/ml) and the plates were incubated for one day at 37 °C, subsequently the addition of 10 µl of resazurin blue dye was done. After 7–12 h, the column showed the appearance of blue and pink colors, pointing out bacterial growth inhibition and bacterial viability, respectively.

2.5.2. Antibiofilm activity of Cr-SeNWs

The biofilm inhibition of Gram-Positive (*S. aureus*, *E. faecalis*) and Gram-negative (*P. aeruginosa, E. coli*) bacteria by Cr-SeNWs were determined by following Divya et al. [52]. Briefly, tested bacterial strains (1×10^6 cfu ml^{-1}) grown on glass pieces (diameter 1 × 1 cm) were placed in 24 well plate along with 1.5 ml of nutrient broth plus various concentration of Cr-SeNWs (50–75 µg/ml) followed by incubation at 37 °C for 48 h. The glass pieces were then bind with crystal violet (0.04%) and observed by a Nikon inverted microscope (ECLIPSE *Ti*100) at 40× magnification. Crystal violet stain bound to tested bacterial biofilm was rinsed using 100% ethanol and quantified by measuring the absorbance at 545 nm using the microplate absorbance reader. Similarly, another set of biofilms was prepared as described above, binding with 0.1% acridine orange and observed through a CLSM (Carl Zeiss LSM 710, Germany) at 20X magnification. The Z-stack examination (three-dimensional architecture) was performed through the Zen 2009 image software (Carl Zeiss, Germany).

2.5.3. Live and dead cell assay post-treatment with Cr-SeNWs

Live and dead cell assay post-treatment with Cr-SeNWs, were done using the BacLight Bacterial Viability Kit (L7012, Invitrogen) following Stiefel et al. [53]. In brief, bacterial cultures of Gram positive (*S. aureus, E. faecalis*) and Gram negative (*P. aeruginosa, E. coli*) were used to obtain suspension density of OD_{600} = 1.2 with fresh nutrient medium and aliquot into 1.5 ml Eppendorf tubes. Cells were treated with two different concentrations of Cr-SeNWs (50 and 75 µg/ml), then incubated at 37 °C for 1 h and centrifuged at 7000 × *g* for 10 min. After, the pellet was washed by PBS buffer. The pellet was combined with nuclear binding stains containing 10 µL of 3 mM SYTO® 9 and 20 µL of 20 mM propidium iodide in 2 ml of PBS buffer, at 37 °C in absence of light for 900 s. The Cr-SeNWs-treated bacterial cells were studied by CLSM.

2.6. Cytotoxicity assays on RBCs

Cr-SeNWs was tested for hemolytic activity according to the method by Abinaya et al. [54]. Goat blood was mixed with1 ml of sodium citrate (9:1) to prevent coagulation. The sample was centrifuged at 3000 × *g* for 10 min, the pellet containing RBCs was washed with 10 ml of PBS (pH = 7.4). RBCs were incubated with PBS and 2 ml of erythrocyte suspension was treated with Cr-SeNWs at various concentrations (1.5, 2.5 and 5.0 mg/ml), PBS was used as control; each suspension was incubated at 37 °C for 1 h. The treated samples were centrifuged and the supernatant was separated. The collected supernatant (2 ml) was used for absorption studies at OD = 540 nm using a UV–vis spectrophotometer and the percentage (%) of hemolysis was estimated:

$$\text{Hemolysis (\%)} = (A_{\text{sample}} - A_{\text{blank}})/A_{\text{control}} \times 100$$

In addition, the treated solution was smear on the glass slide and captured under Nikon inverted light microscopy (Nikon U-RFLT50, Japan) at 40X magnification for visualization of the morphological changes of RBCs.

2.6.1. Morphological studies on RBCs

Morphology study of RBCs was examined by light microscopy (Nikon U-RFLT50, 40X). RBCs were incubated with 1.5, 2.5, 5.0 mg/ml of Cr-SeNWs for 24 h, then the samples were centrifuged. The supernatant was removed then the pellet was washed with PBS for removing unbounded Cr-SeNWs, a drop of suspension was mounted on a glass slide with cover slip and examined under the microscope (Nikon U-RFLT50, Japan, 40X).

2.7. Antioxidant activity of Cr-SeNWs

The antioxidant potential of Cr-SeNWs was determined by DPPH [1, 1-diphenyl-2-picryl hydrazyl] radical method as described by Das et al. [55] with slight modifications. The reaction mixture containing 100 µl of 0.2 Mm DPPH dissolved in 95% methanol (v/v) solution and Cr-SeNWs at various concentrations (i.e., 20, 40, 60, 80 and 100 µg/ml) was added in 96 well microtiter plate. After incubation at 37 °C in the dark for 30 min, the absorbance was calculated at OD = 517 nm. Ascorbic acid was set as positive control, crustin was the negative control. The DPPH radical scavenging ability of Cr-SeNWs, crustin and ascorbic acid was estimated as follows:

$$\text{DPPH scavenging activity (\%)} = (1 - (A_{\text{sample}} - A_{\text{blank}})/A_{\text{control}}) \times 100$$

2.8. Mosquito larvicidal activity of Cr-SeNWs

3rd instar larvae of *Cx. tritaeniorhynchus* and *Cx. quinquefasciatus* were reared as described by Abinaya et al. [54]. On both species, larvicidal activity was studied adopting the WHO method (WHO 1996) [56] with minor changes by Vijayakumar et al. [23]. For each species, each replicate was composed by 20 mosquito larvae plus 200 ml of water. Different concentrations of Cr-SeNWs (i.e., 2, 4, 6, 8, 10 mg/l) were evaluated. The control was dechlorinated tap water. After 24 h of exposure, the number of dead larvae was counted and mortality (%) was reported as the average of 3 replicates. Control mortality was corrected by using Abbott's formula and the mortality (%) was calculated.

2.8.1. Microscopic and histological studies on mosquitoes post-exposure to Cr-SeNWs

Microscopic studies were done as described by Song et al. [57] with slight modifications, 3rd instar larvae of both species Cr-SeNWs treated and control were fixed 10% formalin on slide along with propidium iodide (PI) staining to understand the effect of physical adsorption and internalization of Cr-SeNWs on *Cx. quinquefasciatus* and *Cx. tritaeniorhynchus*, the uptake of Cr-SeNWs was visualized using fluorescent dye propidium iodide staining in CLSM by fluorescent and PMT mode

(Carl Zeiss, Germany).

Furthermore, 3rd instar larvae of both species Cr-SeNWs treated and control were fixed and mounted in paraffin blocks with 8 µm thick sections of larval tissue. They were cut with glass knives using a rotary microtome and mounted on glass slides. The sections were treated with haematoxylin and eosin stains for histopathological analysis and then observed using the photomicroscope Nikon SMZ 745 T Japan and light microscopy [54].

2.9. Statistical analysis

Mosquito larval mortality data were subjected to probit analysis and LC_{50}, LC_{90} values were calculated. Data normality was checked through the Shapiro-Wilk test ($P > 0.05$). Microbial pathogen growth inhibition data and antioxidant assays were examined by ANOVA followed by Tukey's HSD test. We employed the software SPSS version 21. In all experimental data analyses, $P < 0.05$ was considered as statistically significant to assess the differences among control and treated groups.

3. Results

3.1. Synthesis and characterization of Cr-SeNWs

In the present investigation, Cr-SeNWs were synthesized using the antimicrobial peptide crustin from *P. pelagicus* crabs, which acts as the capping agent for the fabrication of nanowires. After 2-hours incubation period, color changed from transparent to fire red. The observed color change was due to the reduction of sodium selenite to form selenium nanowires. Below the chemical reaction and mechanism of sodium selenite to form selenium nanowires, thus confirming the synthesis of Cr-SeNWs.

Sodium selenite + Crustin + Ascorbic acid→Crustin capped selenium nanowires (Cr-SeNWs)

$$Na_2SeO_3 + Cr + C_6H_8O_6 \rightarrow Se^{\circ} \rightarrow \text{Cr-SeNWs}$$

Basic optical properties of Cr-SeNWs were studied using UV–Vis absorption spectroscopy. An absorbance peak (λ max) at 350 nm was recorded, due to surface Plasmon resonance (SPR) (Fig. 1A).

XRD peaks recorded herein well matched with the standard selenium (JCPDS file no.65-1290). Diffraction peaks were observed 2θ value at 12° and 28° these peaks correspond to (020) and (241) lattice planes, respectively (Fig. 1B). No additional diffraction peaks were observed, indicating the presence of pure monocline Cr-SeNWs.

Concerning FTIR spectrum, the broad peak at 3442.52 cm^{-1} corresponded to N-H stretching vibrations of primary amide group of crustin; the intense band at 2922.38 cm^{-1} indicated the presence of alkynes (C≡C), while the strong peak at 1633.33 cm^{-1} represented the diketones group. The peak at 1380.56 cm^{-1}indicated the isopropyl group, while other peaks showed C═O stretching vibrations, OH and carboxylic groups in agreement with the standard peaks of selenium, due to the stretching of Se bonds (Fig. 1C).

HR-TEM, SEM and SAED pattern shed light on the nano-crystalline nature of Cr-SeNWs. SAED diffraction results (Fig. 2) support the XRD pattern described above. Cr-SeNWs showed wires-like shape with size ranging from 17 to 47 nm (Fig. 2). The Raman spectrum of Cr-SeNWs was recorded and the peak band centered, then obtaining two peaks, one at 1871 cm^{-1}in G mode and the other in E00 mode at 1600 cm^{-1} D mode (Fig. 3A). The elemental composition of Cr-SeNWs was outlined by EDAX analysis demonstrating that the Se elemental composition was 57% (Fig. 3B).

3.2. Antibacterial activity of Cr-SeNWs

Cr-SeNWs inhibited the growth of Gram positive and Gram negative bacteria. The inhibition zone was higher in Gram positive than in gram negative bacteria depicted in Table 1. Cr-SeNWs showed higher antimicrobial activity on Gram-positive bacteria (*S. aureus*, *E. faecalis)* over Gram-negative ones (*P. aeruginosa*, *E. coli)*. The zone of inhibition was larger on *S. aureus* (50 µg/ml = 4.0 mm, 75 µg/ml = 7.2 mm) and *E. faecalis* (50 µg/ml = 3.1 mm, 75 µg/ml = 5.1 mm), over *P. aeruginosa* (50 µg/ml = 2.1 mm, 75 µg/ml = 4.8 mm), *E. coli* (50 µg/ml = 1.3 mm, 75 µg/ml = 4.3 mm) bacteria. Significant differences were detected testing increasing concentrations of Cr-SeNWs on the targeted microbial pathogens (*S. aureus:* $F_{2,6} = 828.1$, $P < 0.001$, *E. faecalis:* $F_{2,6} = 1.80e3$, $P < 0.001$, *P. aeruginosa* $F_{2,6} = 84.246$, $P < 0.001$, *E. coli:* $F_{2,6} = 774.4$, $P < 0.001$).

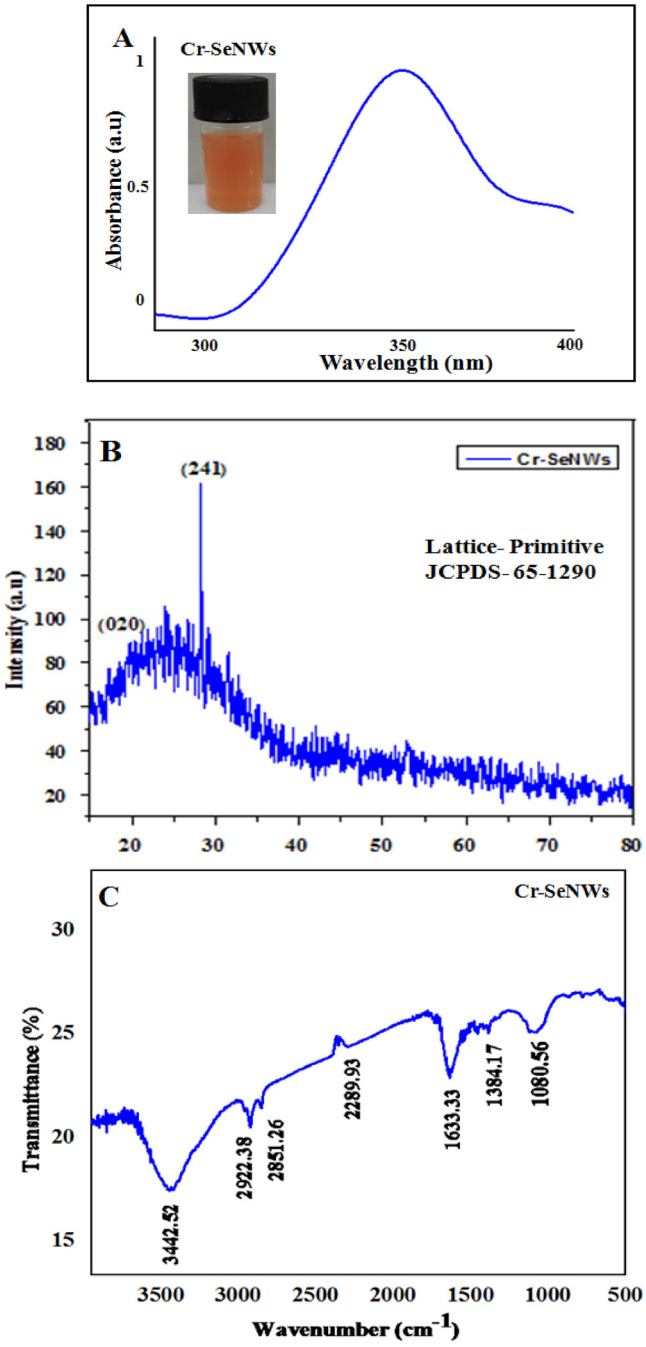

Fig. 1. [A] UV–Visible spectrum of crustin-synthesized selenium nanowires (Cr-SeNWs) highlighting an absorption peak at 350 nm. [B] XRD pattern of Cr-SeNWs. [C] FTIR spectrum showing the functional groups characterizing Cr-SeNWs.

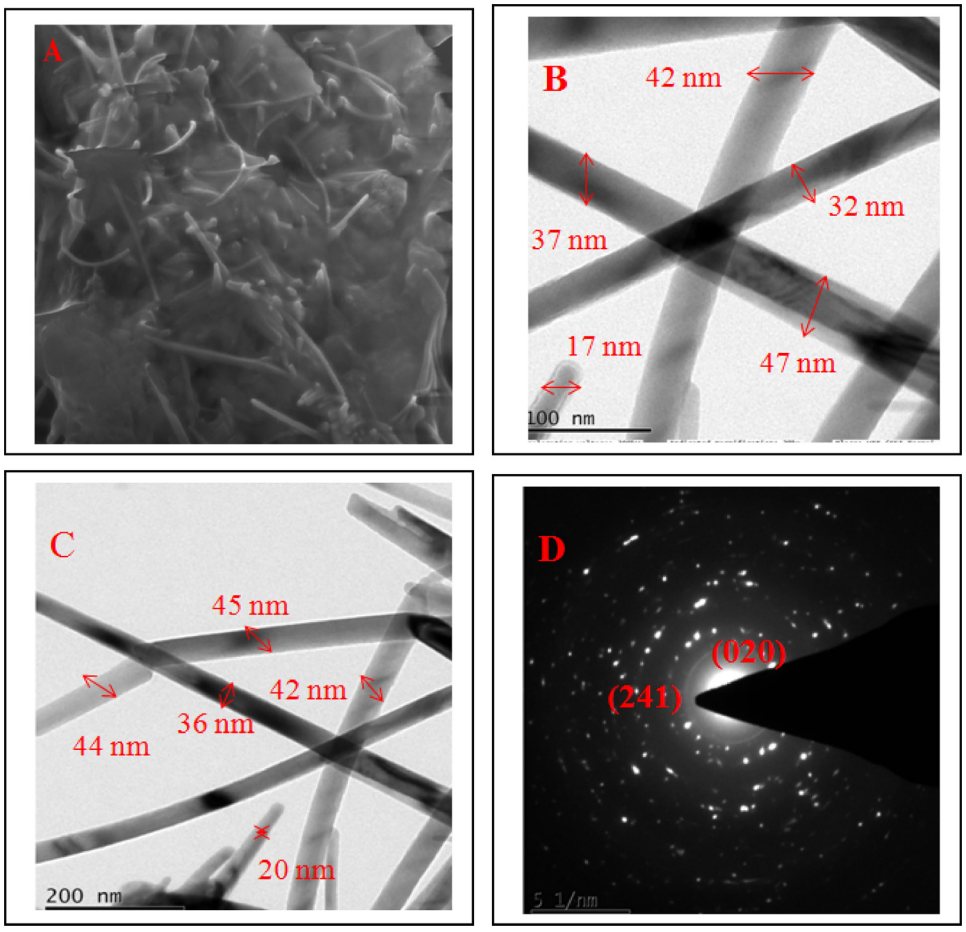

Fig. 2. [A] SEM of crustin-synthesized selenium nanowires (Cr-SeNWs). [B–C] HR-TEM analysis of Cr-SeNWs. [D] SAED pattern of Cr-SeNWs.

3.2.1. Microtiter plate assay for MIC with resazurin dye

Bacterial control of Gram-positive and Gram-negative species was achieved testing10 µg/ml and 100 µg/ml of Cr-SeNWs, respectively. The MIC value was determined by the disappearance of color change occurring at lowest effective concentration. In this assay, pink showed bacterial growth while blue indicated the bacterial growth arrest, as a result, MIC < 25 µg/ml showed high antibacterial activity of Cr-SeNWs against targeted bacterial pathogens (data not shown).

3.2.2. Antibiofilm activity of Cr-SeNWs

In the present study, inverted microscope and CLSM bacterial observation showed high thickness biofilm formation in control. Gram-positive bacteria (*S. aureus*, *E. faecalis*) and Gram-negative bacteria (*P. aeruginosa*, *E. coli*) whereas, bacteria treated with Cr-SeNWs (50 and 75 µg/ml) showed inhibited biofilm formation in a concentration-dependent manner. At the highest Cr-SeNWs concentration tested (75 µg/ml) biofilm growth was completely arrested (Fig. 4).

3.2.3. Live and dead assay on bacteria treated with Cr-SeNWs

Post-treatment with Cr-SeNWs, tested bacteria showed reduced growth inhibition as depicted by CLSM analysis using nuclear membrane permeable staining. Control cells showed a higher quantity of live cells (green color, SYTO® 9) in Cr-SeNWs treated dead cells are (red color, propidium iodide) dominated, if compared to live cells, at both 50 and 75 µg/ml (Fig. 5).

3.3. Cytotoxicity test on RBCs

The hemolytic potential noted on RBCs treated with Cr-SeNWs at different concentrations was reported in Table 2. RBCs exposed to Cr-SeNWs (1.5, 2.5 and 5.0 mg/ml) showed a significant effect of the tested concentration ($F_{3,9} = 6.429$, $P = 0.016$). Trials showing the interaction of Cr-SeNWs (5.0 mg/ml) with RBCs revealed low hemolytic activity on RBCs. Hence, these concentrations of Cr-SeNWs are considered biocompatible for biomedical purposes (Table 2).

3.3.1. Morphological changes on RBCs

The inverted microscopic images of RBCs treated with 1.5, 2.5 and 5.0 mg/ml of Cr-SeNWs, were taken after an incubation period of 24 h (Fig. 6a). When compared to control RBCs (Fig. 6a), scarce membrane damage and structural deformation at the tested concentration level were noted.

3.4. Antioxidant activity of Cr-SeNWs

The antioxidant activity of Cr-SeNWs was studied testing ascorbic acid as positive control and crustin as negative control. The scavenging activity of Cr-SeNWs increased raising the tested concentration, i.e., 25, 50, 75 and 100 µg ml^{-1}. The effect of testing increasing concentrations of ascorbic acid ($F_{4,16} = 499.4$, $P < 0.001$), Cr-SeNWs ($F_{4,16} = 4.488$, $P < 0.001$) and crustin ($F_{4,16} = 3.002$, $P < 0.001$) was significant. As expected, maximum scavenging activity of Cr-SeNWs was showed testing 90 ± 1.2% at 100 µg/ml (Fig. 6b). Overall, the scavenging activity of Cr-SeNWs was limited concerning the scavenging potential on DPPH, if compared to the positive control.

3.5. Mosquito larvicidal activity of Cr-SeNWs

The larvicidal activity of Cr-SeNWs against late 3rd instar larvae of *Cx. quinquefasciatus* and *Cx. tritaeniorhynchus* was reported in Table 3.

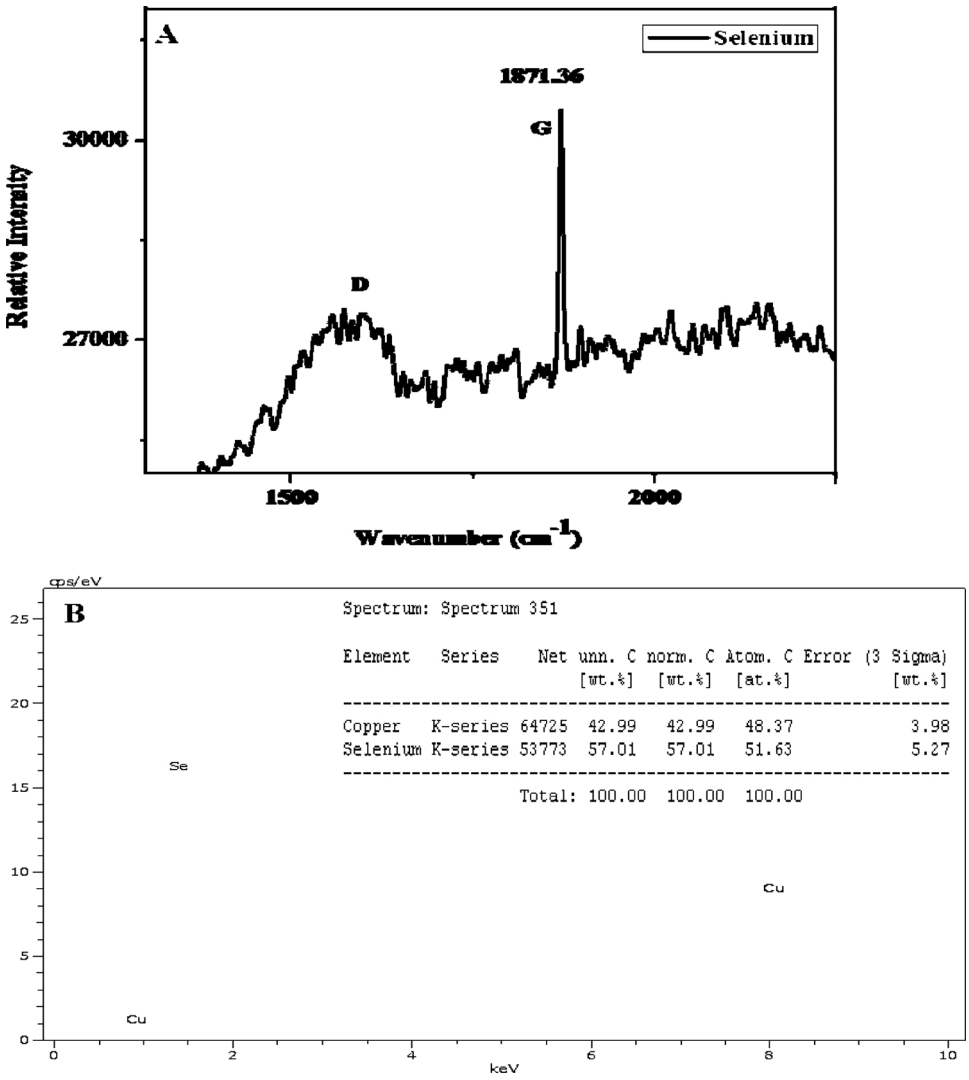

Fig. 3. [A] Raman scattering spectrum and [B] EDAX analysis of crustin-synthesized selenium nanowires (Cr-SeNWs).

Table 1
Growth inhibition activity of crustin-synthesized selenium nanowires (Cr-SeNWs) against Gram-positive and Gram-negative bacteria.

Bacteria	Accession number	Zone of inhibition (mm)	
		50 µg ml^{-1}	75 µg ml^{-1}
Staphylococcus aureus	MTCC-9542	4.0 ± 0.2^{a}	7.2 ± 0.4^{b}
Enterococcus faecalis	HQ693279.1	3.1 ± 0.1^{a}	5.1 ± 0.4^{b}
Escherichia coli	ATCC 25922	1.3 ± 0.3^{a}	4.3 ± 1.1^{b}
Pseudomonas aeruginosa	HQ 4006631	2.1 ± 0.2^{a}	4.8 ± 1.2^{b}

Within each row, different letters indicate a significant effect of the tested concentration ($P < 0.05$).

In both species, mosquito mortality raised when increasing the tested concentration of Cr-SeNWs (Supplementary Online Material Fig. S1). 100% mortality of *Cx. quinquefasciatus* and *Cx. tritaeniorhynchus* larvae was achieved testing Cr-SeNWs at 10 mg/L. The LC_{50} and LC_{90} values of Cr-SeNWs against *Cx. quinquefasciatus* were 4.15 mg/l and 8.61 mg/l respectively. The LC_{50} and LC_{90} values of Cr-SeNWs on *Cx. tritaeniorhynchus* were 4.85 mg/l and 9.53 mg/L respectively in Table 3.

3.5.1. CLSM studies on mosquito larvae exposed to Cr-SeNWs

Microscopy analyses showed that Cr-SeNWs were ingested by the larvae of both tested *Culex* species, leading to nanowire accumulation in the abdominal tissues. At higher concentrations, deposited Cr-SeNWs were noted as attached to the body surface of *Culex* larvae, also leading to reduced swimming ability. CLSM visualization on nanowire-exposed mosquito larvae highlighted live cells marked by green fluorescence, while dead cells are outlined by red fluorescence (Fig. 7). Control larvae of both *Cx. quinquefasciatus* and *Cx. tritaeniorhynchus* showed strong green fluorescence, indicating that the body cells were live (Fig. 7). On the other hand, *Cx. quinquefasciatus* and *Cx. tritaeniorhynchus* larvae treated with Cr-SeNWs at 10 mg/L mostly showed red fluorescence in head, thorax and abdomen regions, indicating that a high number of body cells were dead (Fig. 7A and B). This is due to the permeability of PI dye toward larvae with damaged body cell membranes.

3.5.2. Histopathological studies on Cr-SeNWs-treated mosquito larvae

Histological studies were also carried out on nanowire-exposed *Cx. quinquefasciatus* and *Cx. tritaeniorhynchus* larvae (Fig. 8), since both target species showed 100% mortality at extremely low concentrations of Cr-SeNWs. Larvae treated with Cr-SeNWs showed significant histological changes over control. Noted damages in Cr-SeNWs-treated larvae included the loss of antennal, lateral, upper and lower head hairs, breakdown of epithelial layer and outer cuticle, the hindgut and muscles were also affected, the epithelium was vacuolated within the cellular membrane damages, but still enclosing the cell nuclei (Fig. 8).

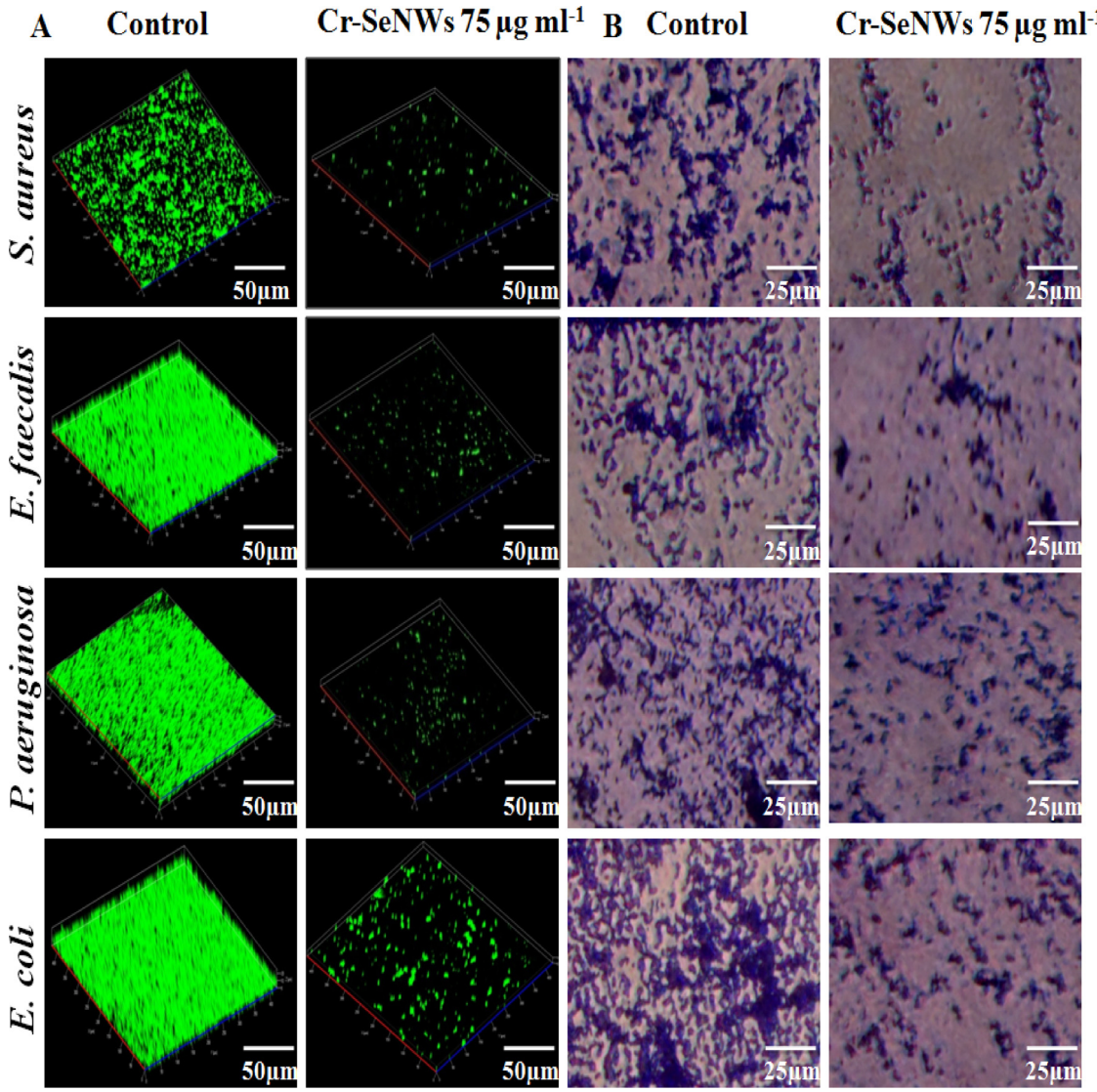

Fig. 4. Antibiofilm activity of crustin-synthesized selenium nanowires (Cr-SeNWs) against Gram-positive and Gram-negative bacteria. (A) Confocal laser scanning microscopy. (B) Light microscopy.

4. Discussion

From a biological point of view, several trace elements play a key role on life, such as selenium, which is widely used in the production of food products as well as by biotechnology and pharmaceutical industries. Quantitatively trace amount of selenium may represent useful supplements leading to proper functioning in various living organisms [58]. For example, trace amounts of selenium binds and produce selenium-rich organisms like yeast *Saccharomyces cerevisiae* and *Candida albicans* exploited by several industrial applications [59,60]. The present research firstly reports the successful synthesis of selenium nanowires (Cr-SeNWs) using purified crustin in the presence of ascorbic acid. Bioactive antimicrobial peptides (AMPs) are an interesting class of bio-pharmaceuticals released from proteins that exhibit unique properties, including – besides antibacterial and antifungal activity – even antioxidant and antihypertensive [61]. During the last decades, organometallic groups in biological molecules like peptides and proteins received a major research focus. The metal core can be responsible of bio-functionalities, including the growth inhibition against multidrug-resistant bacteria [62]. The development of effective and cheap purification processes to obtain AMP from the mass of proteins in the circulating haemolymph is therefore crucial [63] since these molecules can combine with several molecules like carbohydrates by non-self-recognition reactions [64]. In this framework, earlier antimicrobial peptide/protein-based preparation of nanoparticles, such as zinc oxide nanoparticles with β-1, 3-glucan binding protein (BGBP) from *Paratelphusa hydrodromus* [28] and nanosilver capped with BGBP and lectin from *Portunus pelagicus,* have been reported [29,64]. However, the invertebrate biomolecule-based fabrication of selenium nanostructures for antimicrobial and insecticidal purposes has not been studied. On the other hand, selenium nanowires prepared using *Shinorhizobial* cyclosophoraose (cyclic b-(1→2)-glucan) and ascorbic acid have been reported [65].

The various mechanism of reduction selenate to selenite ($SeO_4^{-2} \rightarrow SeO_3^{-2}$), selenite into Selenium ($SeO_3^{-2} \rightarrow Se^0$) seems to vary among different micro-organisms, as well as among different enzymes [66]. The reduction of inorganic selenium using glutathione was reported by Avendano et al., (2016) [66]. The reduction of selenite to selenium, $SeO_3^{-2} \rightarrow Se^{\circ}$ can be explained by the following mechanism (*i*) selenite becomes chelated first by thiol-containing molecules like glutathione, as of selenodiglutathione; (*ii*) this compound is the substrate of glutathione as an enzyme reductase that produces unbalanced intermediates ultimately transformed to elemental selenium. Hence, the current synthesis of selenium nanowires capped with crustin molecule

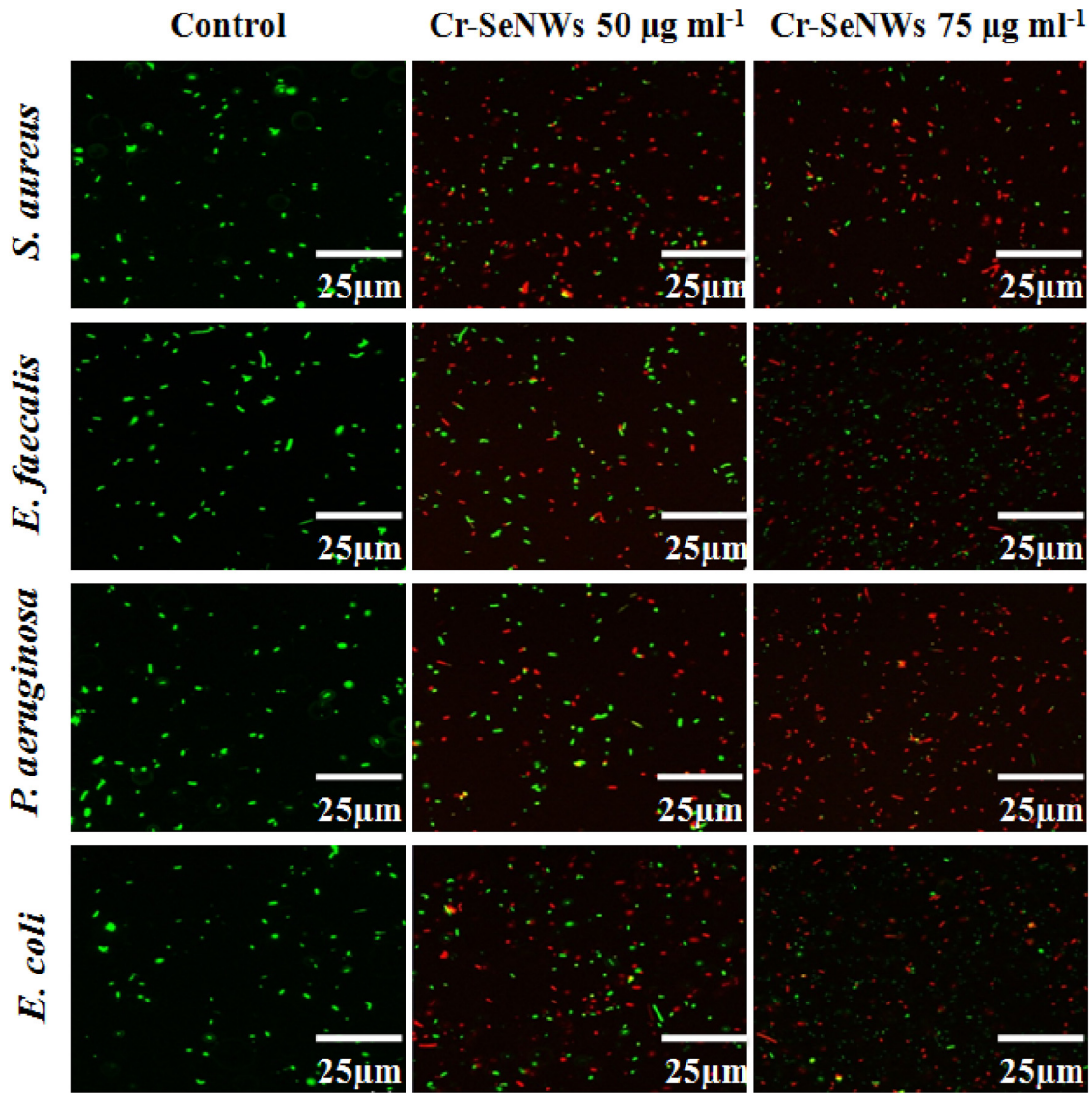

Fig. 5. Live and dead cell assay testing crustin-synthesized selenium nanowires (Cr-SeNWs) against Gram-positive and Gram-negative bacteria.

Table 2
Hemolytic activity of crustin-synthesized selenium nanowires (Cr-SeNWs).

Treatment	Optical density at 540nm	Hemolysis (%)
Control (saline)	1.209 ± 0.004	–
Cr-SeNWs 1.5 mg	0.011 ± 0.002	0.94 ± 0.12[a]
Cr-SeNWs 2.5 mg	0.014 ± 0.003	1.16 ± 0.25[ab]
Cr-SeNWs 5mg	0.018 ± 0.002	1.52 ± 0.18[b]

Within each column, different letters indicate significant differences ($P < 0.05$).

was obtained through the reduction of sodium selenite into selenium. Preliminarily confirmation was obtained noting the color change to red due to the reduction of selenite into elemental selenium. These results are supported by Kieliszek et al. [67] who reported that the employ of glucose might enhance a reduction of selenium occurring in the form of selenite ions, which led to in the formation of red elemental selenium.

Herein, the synthesis Cr-SeNWs was confirmed by UV spectroscopy with an absorption peak obtained at 350 nm. Earlier studies showed that the selenium nanostructure absorption peak can be detected at 254 nm and 374 nm [68]. X-ray diffraction analysis pointed out the crystalline nature of synthesized monoclinic Cr-SeNWs, substantiating the arrangement of atoms and lattice nature with different Bragg's reflection peaks at 12° and 28°, in agreement with Gao et al. and Shah et al. [69,70]. The FTIR spectrum of crustin was recently reported by our recent study Rekha et al. [71]. Current research showed that Cr-SeNWs resulted in strong bands indicating the presence of NH, C═O, C≡C, OH and carboxylic groups. These results strongly suggested the interaction between the cysteine-rich peptide with selenium nanowires [72].

Structure prediction of selenium nanowires smooth surface with sharp edges was obtained by SEM analysis and the results correlated with Li et al. [73], who also synthesized selenium nanocomposites. HR-TEM showed single nanowires with dark strips depicting crystalline nature. Moreover, Raman spectroscopy showed a peak range indicating the presence of pure selenium. This outcome supports the earlier research by Ali et al. [74]. EDAX analysis of Cr-SeNWs showed a significant selenium peak (57%) concluding that selenium was highly presented in the prepared sample.

AMPs play an essential role in drug development for pharmaceutical applications [75]. Nanoparticles fabricated using biomolecules can be used for various therapeutic applications, due to their multifaceted properties, since they often are biocompatible and eco-friendly in nature. As an example, earlier BGBP-fabricated ZnO nanoparticles showed excellent antibiofilm activity, as reported by Iswarya et al.

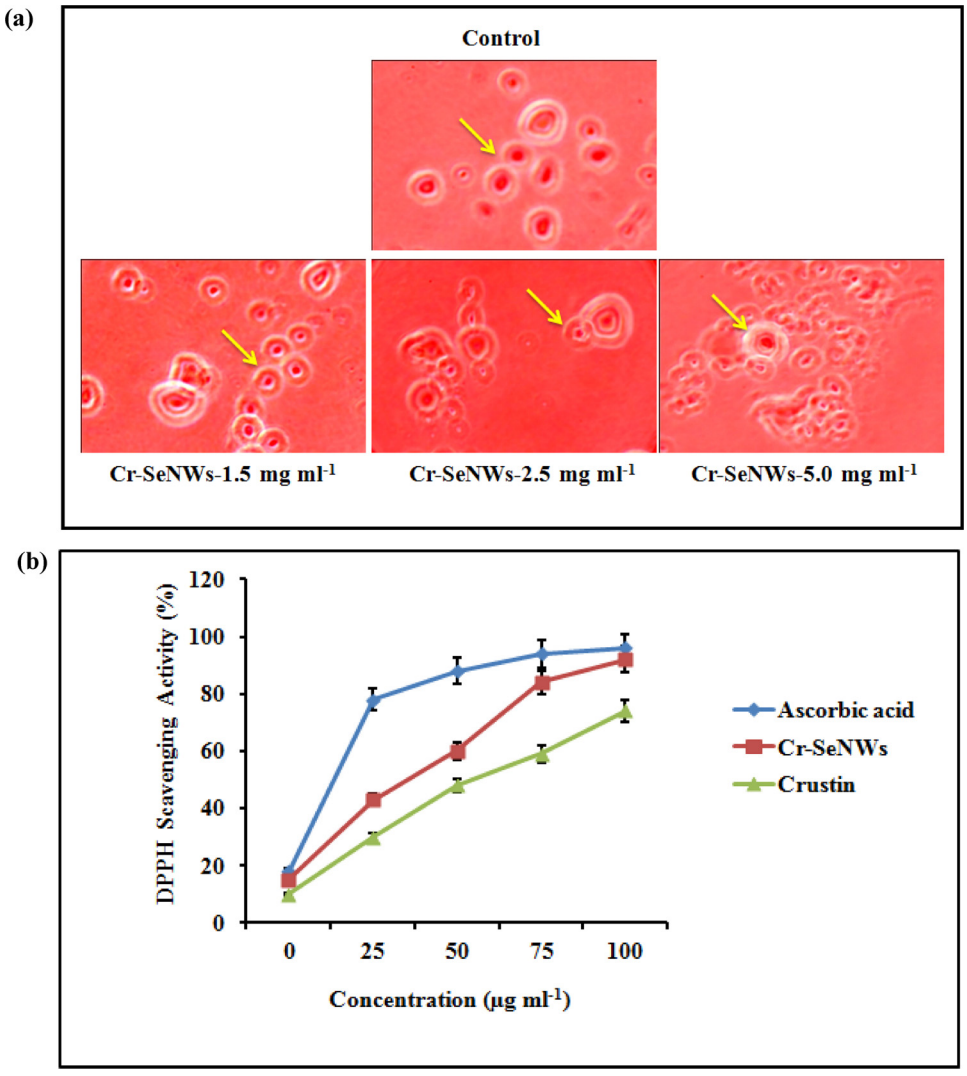

Fig. 6. (a) Hemolytic activity of crustin-synthesized selenium nanowires (Cr-SeNWs) on red blood cells; the arrow (⟶) indicates cell morphology without cell damages. **(b)** Antioxidant activity of Cr-SeNWs. T-bars represent SD. (For interpretation of the references to colour in this figure legend, the reader is referred to the web version of this article).

[28]. Various metal nanoparticles have been studied, with special reference to Ag ones. The antibacterial ability of silver nanowires was examined against *E. coli, S. aureus* and *Bacillus subtilis* [76]. High antibacterial efficacy and relevant membrane damages on various bacteria have been also noted testing 0.7 g/l of magnesium oxide (MgO) nanowires [77]. In another report, selenium nanomaterial was used to inhibit the growth of *S. aureus* [78]. Selenium nanowires and nanotubes also had the ability to reduce the biofilm formation. Nanowires [79–82] and nanotubes [83] have the excellent properties to trap bacteria [84] in bloodstream. Concerning live and dead assays, our results showed high red fluorescent indicating dead cells post-treatment with Cr-SeNWs (50 and 75 µg/ml) over the control. Similarly, Divya et al. [85] outlined that *Scylla serrata* β-GBP at 100 µg/mL allowed high bacterial cell control using BacLight fluorescent staining technique.

in vitro assays testing the hemolytic activity of synthesized Cr-SeNWs exhibited scarcely toxic and non-hemolytic activity on RBC cells treated with Cr-SeNWs at 5.0 mg/ml [54], DPPH scavenging potential was also noted. The total antioxidant potential of Cr-SeNWs was higher

Table 3
Toxicity of crustin-synthesized selenium nanowires (Cr-SeNWs) against larvae of the Japanese encephalitis vectors *Culex quinquefasciatus* and *Culex tritaeniorhynchus*.

Target	Concentration (mg L^{-1})	Mortality (%) ± SD	LC_{50} (95% LCL-UCL)(mg L^{-1})	LC_{90} (95% LCL-UCL)(mg L^{-1})	Regression equation	χ^2 (*d.f.* = 5)
Culex quinquefasciatus	2	31 ± 0.8	4.15	8.61	$y = 13.30 + 8.650x$	$8.708^{n.s}$
	4	48 ± 1.2	(2.26–5.37)	(7.07–12.37)		
	6	64 ± 0.6				
	8	83 ± 0.8				
	10	100 ± 0.0				
Culex tritaeniorhynchus	2	26 ± 0.6	4.85	9.53	$y = 5.50 + 8.950x$	$7.783^{n.s}$
	4	41 ± 0.8	(4.36–5.30)	(8.79–10.52)		
	6	54 ± 0.6				
	8	78 ± 1.2				
	10	97 ± 0.8				

d.f. = degrees of freedom.
$^{n.s.}$ = not significant (α = 0.05).

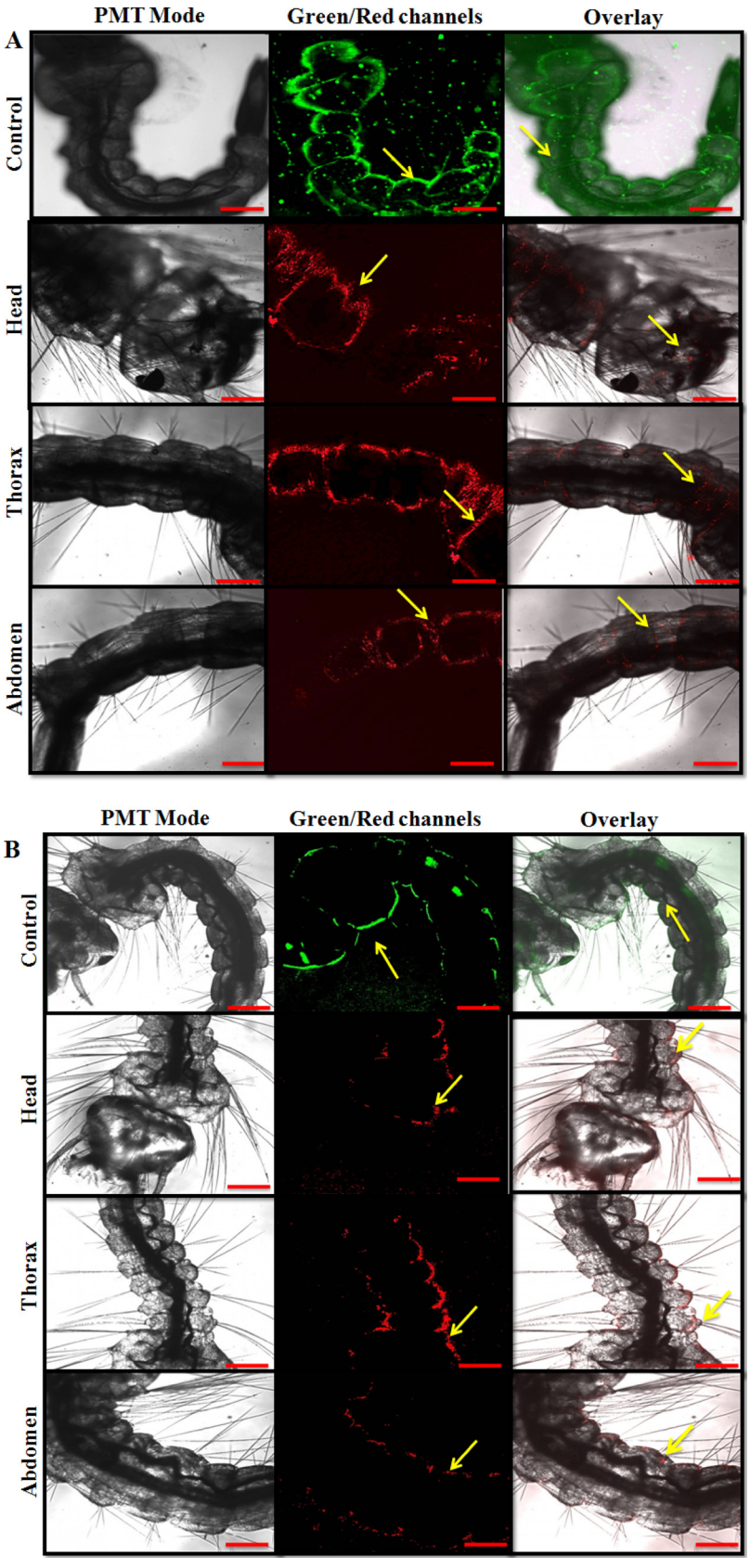

Fig. 7. Confocal laser scanning microscopy of crustin-synthesized selenium nanowires (Cr-SeNWs)-treated larvae of *Culex quinquefasciatus* (A) and *Culex tritaeniorhynchus* (B) (scale bar = 1 mm), the arrow (⟶) highlights live (green) and dead (red) cells. (For interpretation of the references to colour in this figure legend, the reader is referred to the web version of this article).

if compared to crustin results. Earlier studies noted that selenium nanomaterials have higher antioxidant capacity that eliminate and even prevent the formation of free radicals through the increase of the Se-containing enzyme, glutathione peroxidase [86]. As recently pointed out, nanomaterials can achieve toxicity on insects through a wide number of mechanisms of action [26]. Previously, Kieliszek et al., (2018) [60] showed bare selenium toxicity on *Saccharomyces cerevisiae* MYA-2200 and *Candida utilis* ATCC 9950 yeasts. Selenium toxicity

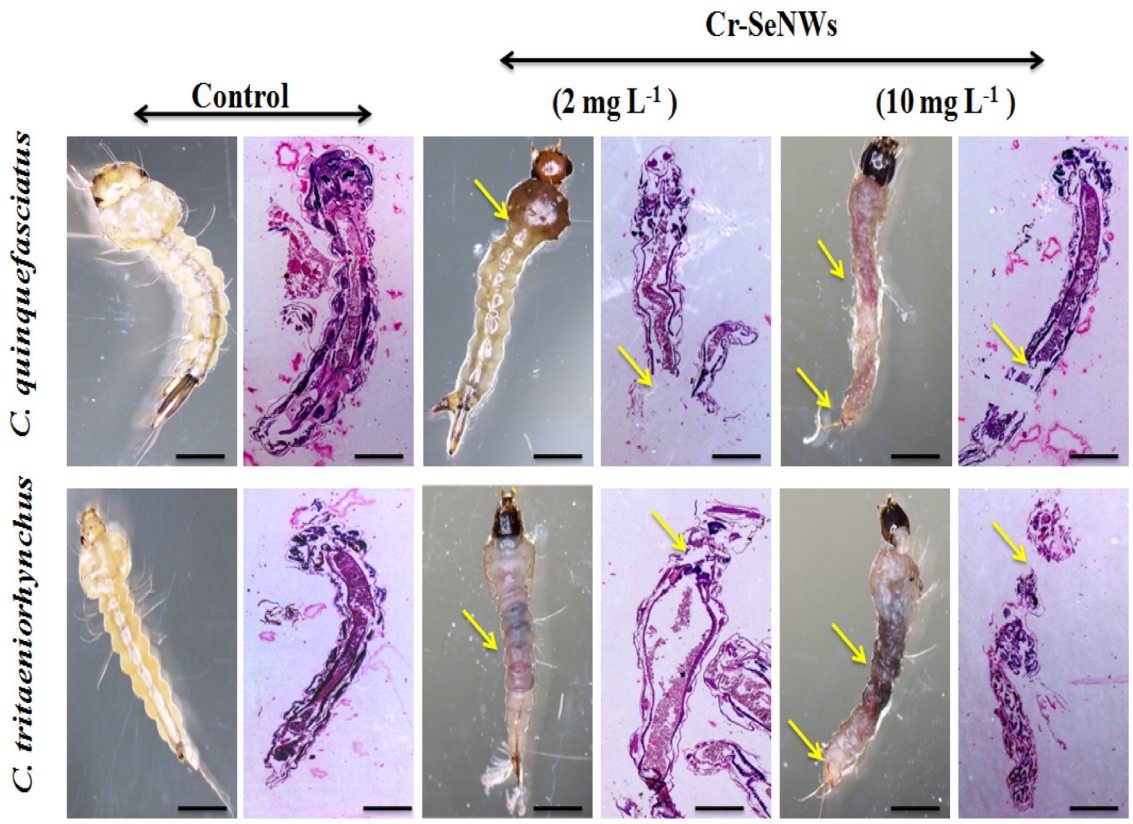

Fig. 8. Photomicroscope and histological analysis of crustin-synthesized selenium nanowires (Cr-SeNWs)-treated **(a)** *Culex quinquefasciatus* and **(b)** *Culex tritaeniorhynchus* larvae. The arrow (⟶) indicates tissue damages to abdomen, thorax and siphon regions (scale bar = 1 mm). (For interpretation of the references to colour in this figure legend, the reader is referred to the web version of this article).

affected the differentiation of cellular morphology, changes in protein level, lipid peroxidation, which consequently damage the loss of integrity of the cytoplasmic membrane in the yeasts cells.

However, the mechanisms triggered by Se nanomaterials leading to mosquito larval death are still poorly understood. We can argue that the Cr-SeNWs can rapidly damages organelles and cellular enzymes, leading to a strong reduction of ATP synthesis and loss of membrane permeability [12]. Results reported here showed higher toxicity against mosquitoes, if compared to earlier studies where nanomaterials (e.g., nanosilver) have been produced using plant extracts or related products [87–90]. For example, Ag nanoparticles obtained using *Pedalium murex* extract were less toxic to mosquitoes, i.e., *Ae. aegypti* LC_{50} = 34.88, LC_{90} = 64.56 µg/ml [91]. On the other hand, zinc oxide nanoparticles produced using the leaf extract *Plectranthus amboinicus* showed a remarkable mosquitocidal activity, both on *Cx. quinquefasciatus,* with LC_{50} = 3.1 mg/L and LC_{90} = 4.5 mg/L, and *Cx. tritaeniorhynchus* is LC_{50} = 4.2 mg/L and LC_{90} = 5.7 mg/L [23]. Herein, larvicidal activity was very high, since Cr-SeNWs tested on both *Culex* species showed interesting results for mosquito control, with effective toxicity on *Cx. quinquefasciatus* i.e., LC_{50} = 4.1 mg/L and LC_{90} = 8.6 mg/L; as well as on *Culex tritaeniorhynchus*, i.e., LC_{50} = 4.8 and LC_{90} = 9.5 mg/L. Comparatively, these results suggest the potential of Cr-SeNWs to develop novel insecticides to be used in the fight against *Culex* spp. at minimum concentrations. In agreement with our results, fluorescent water soluble carbon nanoparticles wsCNPs have been recently used to control *Culex* mosquito larvae testing 0.5 mg/l and 3 mg/l [92]. Herein, mosquito cells were stained by propidium iodide and tissue damages were evaluated under CLSM [93]. In the present study, it has been elucidated that Cr-SeNWs were ingested by the larvae of both *Culex* species, leading to nanowire accumulation in the head, thorax and abdominal tissues. Control larvae of *Cx. quinquefasciatus* and *Cx. tritaeniorhynchus* showed strong green fluorescence intensity, indicating that body cells were live. On the other hand, *Cx. quinquefasciatus* and *Cx. tritaeniorhynchus* larvae treated with Cr-SeNWs at 10 mg/L mostly showed PI staining red fluorescence high intensity in head, thorax and abdomen regions, indicating that a high number of body cells were dead. This is due to the permeability of PI dye in larvae with damaged body cell membranes. Fallon [94] recently reported flow cytometry studies on *Wolbachia*-infected mosquito cells using PI staining. In this case, the increase of PI fluorescence intensity during examination was discussed in relation to changes in properties of the host cell, such as adherence to substrate, cell-cell aggregation, and membrane fragility, which can vary over the course of an experiment.

5. Conclusions

Overall the present research work presented an effective and eco-friendly approach to fabricate Cr-SeNWs using crustin. Cr-SeNWs size ranges from 17 to 47 nm, with smooth surfaces. The biofilm inhibition ability was noted testing the nanowires at 75 µg/ml, light and confocal laser scanning microscopy confirmed the results. Notably, the nanowires exhibited highly effective larvicidal properties against two major Japanese encephalitis vector species (*Cx. quinquefasciatus* LC_{50} = 4.1 and LC_{90} = 8.6; *Culex tritaeniorhynchus* LC_{50} = 4.8 and LC_{90} = 9.5). The nanowire mode of action was investigated through confocal laser scanning microscopy and histological studies. To investigate the potential of this nanomaterial for real-world applications. We also evaluated Cr-SeNWs in hemolytic assays, which showed no cytotoxicity at 5 mg/ml. Besides, higher antioxidant activity at the concentration at 100 µg/ml was noted, if compared with purified crustin. The strong antioxidant potential of this nanomaterial can be helpful to boost the shelf-life potential of Cr-SeNWs-based pesticides and antimicrobials. Further studies will be taken to develop Cr-SeNWs as potential mosquito repellents for industrial purposes. In addition, the Cr-SeNWs may

be exploited to produce sterile, clinical biomaterial for bio-pharmaceutical applications.

Conflict of interest

We wish to confirm that there are no known conflicts of interest associated with this publication.

Acknowledgements

This work was supported by the Department of Biotechnology (DBT), New Delhi, India, under the Project grants code BT/PR7903/AAquote/ 3/638/2013. The authors extend their appreciation to the Deanship of Scientific Research at King Saud University for funding this work through Research Group No. RG-1438- 091.

Appendix A. Supplementary data

Supplementary material related to this article can be found, in the online version, at doi:https://doi.org/10.1016/j.jtemb.2018.10.017.

References

[1] G. Benelli, M.F. Duggan, Management of arthropod vector data – social and ecological dynamics facing the one health perspective, Acta Trop. 182 (2018) 80–91.
[2] M.N. Naqqash, A. Gokçe, A. Bakhsh, M. Salim, Insecticide resistance and its molecular basis in urban insect pests, Parasitol. Res. 115 (2016) 1363–1373.
[3] M. Govindarajan, G. Benelli, Facile biosynthesis of silver nanoparticles using *Barleria cristata*: mosquitocidal potential and biotoxicity on three non-target aquatic organisms, Parasitol. Res. 115 (2016) 925–935.
[4] G. Benelli, J. Beier, Current vector control challenges in the fight against malaria, Acta Trop. 174 (2017) 91–96.
[5] G. Benelli, H. Mehlhorn, Declining malaria, rising dengue and Zika virus: insights for mosquito vector control, Parasitol. Res. 115 (2016) 1747–1754.
[6] G. Benelli, D. Romano, Mosquito vectors of Zika virus, Entomol. Gen. 36 (4) (2017) 309–318.
[7] P. Karthika, C. Vadivalagan, D. Thirumurugan, R.R. Kumar, K. Murugan, G. Benelli, DNA barcoding of five Japanese encephalitis mosquito vectors (*Culex fuscocephala, Culex gelidus, Culex tritaeniorhynchus, Culex pseudovishnui* and *Culex vishnui*), Acta Trop. 183 (2018) 84–91.
[8] WHO, Japanese Encephalitis, Fact sheet No 386, Geneva, 2014.
[9] R. Pavela, History, presence and perspective of using plant extracts as commercial botanical insecticides and farm products for protection against insects–a review, Plant Prot. Sci. 52 (2016) 229–241.
[10] T.K. Barik, R. Kamaraju, A. Gowswami, Silica nanoparticle: a potential new insecticide for mosquito vector control, Parasitol. Res. 111 (2012) 1075–1083.
[11] G. Benelli, Research in mosquito control: current challenges for a brighter future, Parasitol. Res. 114 (2015) 2801–2805.
[12] G. Benelli, Commentary: data analysis in bionanoscience—issues to watch for, J. Cluster Sci. 28 (2017) 11–14.
[13] G. Benelli, R. Pavela, Repellence of essential oils and selected compounds against ticks – a systematic review, Acta Trop. 179 (2018) 47–54.
[14] G. Benelli, Gold nanoparticles – against parasites and insect vectors, Acta Trop. 178 (2018) 73–80.
[15] G. Benelli, Plant-borne compounds and nanoparticles: challenges for medicine, parasitology and entomology, Environ. Sci. Poll. Res. 25 (2018) 10149–10150.
[16] M.B. Isman, A renaissance for botanical insecticides, Pest Manage. Sci. 71 (2015) 1587–1590.
[17] M.B. Isman, Bridging the gap: moving botanical insecticides from the laboratory to the farm, Ind. Crops Prod. 110 (2017) 10–14.
[18] B. Banumathi, B. Vaseeharan, R. Periyannan, N.M. Prabhu, P. Ramasamy, K. Murugan, A. Canale, G. Benelli, Exploitation of chemical, herbal and nano-formulated acaricides to control the cattle tick, *Rhipicephalus (Boophilus) microplus* – a review, Vet. Parasitol. 244 (2017) 102–110.
[19] C. Kamaraj, G. Balasubramani, C. Siva, M. Raja, V. Balasubramanian, R.K. Raja, S. Tamilselvan, G. Benelli, P. Perumal, Ag nanoparticles synthesized using β-caryophyllene isolated from *Murraya koenigii*: antimalarial (*Plasmodium falciparum* 3D7) and anticancer activity (A549 and HeLa cell lines), J. Clust. Sci. 28 (2017) 1667–1684.
[20] G. Benelli, R. Pavela, Beyond mosquitoes – essential oil toxicity and repellency against bloodsucking insects, Ind. Crops Prod. B 117 (2018) 382–392.
[21] R. Pavela, F. Maggi, G. Lupidi, H. Mbuntcha, V. Woguem, H.M. Womeni, L. Barboni, L.A. Tapondjou, G. Benelli, *Clausena anisata* and *Dysphania ambrosioides* essential oils: from ethno-medicine to modern uses as effective insecticides, Environ. Sci. Poll. Res. 25 (2018) 10493–10503, https://doi.org/10.1007/s11356-017-0267-9.
[22] J.J. Harrison, H. Ceri, R.J. Turner, Multimetal resistance and tolerance in microbial biofilms, Nat. Rev. Microbiol. 5 (2007) 928.
[23] S. Vijayakumar, G. Vinoj, B. Malaikozhundan, S. Shanthi, B. Vaseeharan, *Plectranthus amboinicus* leaf extract mediated synthesis of zinc oxide nanoparticles and its control of methicillin resistant *Staphylococcus aureus* biofilm and blood sucking mosquito larvae, Spectrochim. Acta Mol. Biomol. Spectrosc. 137 (2015) 886–891.
[24] P.Y. Chung, R. Khanum, Antimicrobial peptides as potential anti-biofilm agents against multidrug resistant bacteria, J. Microbiol. Immunol. Infect. 504 (2017) 405–410.
[25] S. Skalickova, V. Milosavljevic, K. Cihalova, P. Horky, L. Richtera, V. Adam, Perspective of selenium nanoparticles as a nutrition supplement, Nutrition 33 (2017) 83–90.
[26] G. Benelli, Mode of action of nanoparticles against insects, Environ. Sci. Poll. Res. 25 (2018) 12329–12341.
[27] O.S. Oluwafemi, N. Revaprasadu, O.O. Adeyemi, A facile "green" synthesis of ascorbic acid-capped ZnSe nanoparticles, Colloids Surf. B Biointerfaces 79 (2010) 126–130.
[28] A. Iswarya, B. Vaseeharan, M. Anjugam, B. Ashokkumar, M. Govindarajan, N.S. Alharbi, S. Kadaikunnan, J.M. Khaled, G. Benelli, Multipurpose efficacy of ZnO nanoparticles coated by the crustacean immune molecule β-1, 3-glucan binding protein: toxicity on HepG2 liver cancer cells and bacterial pathogens, Colloids Surf. B Biointerfaces 158 (2017) 257–269.
[29] M. Anjugam, B. Vaseeharan, A. Iswarya, M. Divya, N. Marimuthu Prabhu, K. Sankaranarayanan, Biological synthesis of silver nanoparticles using β-1, 3 glucan binding protein and their antibacterial, antibiofilm and cytotoxic potential, Microb. Pathog. 115 (2018) 31–40.
[30] D.I. Andersson, D. Hughes, J.Z. Kubicek-Sutherland, Mechanisms and consequences of bacterial resistance to antimicrobial peptides, Drug Resist. Updat. 26 (2016) 43–57.
[31] J. Sivakamavalli, R. Nirosha, B. Vaseeharan, Purification and characterization of a cysteine- rich 14-kDa antibacterial peptide from the granular hemocytes of mangrove crab *Episesarma tetragonum* and its anti-biofilm activity, Appl. Biochem. Biotechnol. J. 176 (2015) 1084–1101.
[32] K.S. Sruthy, A. Nair, P. Jayesh, S.P. Antony, I.S.B. Singh, R. Philip, Molecular cloning, recombinant expression and functional characterization of an antimicrobial peptide, Crustin from the Indian white shrimp, *Fenneropenaeus indicus*, Fish Shellfish Immunol. 71 (2017) 83–94.
[33] M.P. Rayman, The importance of selenium to human health, Lancet 356 (2000) 233–241.
[34] M. Kieliszek, S. Błażejak, Selenium: significance, and outlook for supplementation, Nutrition 29 (2013) 713–718.
[35] M. Kieliszek, S. Błażejak, Current knowledge on the importance of selenium in food for living organisms: a review, Molecules 21 (2016) 609.
[36] B. Yu, Y. Zhang, W. Zheng, C. Fan, T. Chen, Positive surface charge enhances selective cellular uptake and anticancer efficacy of selenium nanoparticles, Inorg. Chem. 51 (2012) 8956–8963.
[37] W. Liu, X. Li, Y.S. Wong, W. Zheng, Y. Zhang, W. Cao, T. Chen, Selenium nanoparticles as a carrier of 5-fluorouracil to achieve anticancer synergism, ACS Nano 6 (2012) 6578–6591.
[38] J. Fleming, A. Ghose, P.R. Harrison, Molecular mechanisms of cancer prevention by selenium compounds, Nutr. Cancer 40 (2001) 42–49.
[39] S.K. Torres, V.L. Campos, C.G. Leon, S.M. Rodriguez-Llamazares, S.M. Rojas, M. Gonzalez, C. Smith, M.A. Mondaca, Biosynthesis of selenium nanoparticles by *Pantoea agglomerans* and their antioxidant activity, J. Nanopart. Res. 14 (2012) 1–9.
[40] L. Rao, Y. Ma, M. Zhuang, T. Luo, Y. Wang, A. Hong, Chitosan-decorated selenium nanoparticles as protein carriers to improve the in vivo half-life of the peptide therapeutic BAY 55-9837 for type 2 diabetes mellitus, Int. J. Nanomed. 9 (2014) 4819–4828.
[41] H. Wang, J. Zhang, H. Yu, Elemental selenium at nano size possesses lower toxicity without compromising the fundamental effect on selenoenzymes: comparison with selenomethionine in mice, Free Radic. Biol. Med. 42 (2007) 1524–1533.
[42] Y. Zhang, J. Wang, L. Zhang, Creation of highly stable selenium nanoparticles capped with hyperbranched polysaccharide in water, Langmuir 26 (2010) 17617–17623.
[43] K. Kalishwaralal, S. Jeyabharathi, K. Sundar, A. Muthukumaran, Sodium selenite/selenium nanoparticles (SeNPs) protect cardiomyoblasts and zebrafish embryos against ethanol induced oxidative stress, J. Trace Elem. Med. Biol. 32 (2015) 135–144.
[44] A. Abdelouas, et al., Using cytochrome c, to make selenium nanowires, Chem. Mater. 12 (2000) 1510–1512.
[45] B. Zhang, et al., Biomolecule-assisted synthesis of single-crystalline selenium nanowires and nanoribbons via a novel flake-cracking mechanism, Nanotechnology 17 (2006) 385–390.
[46] M. Teimouri, F.K. Nejad, F. Attar, A.A. Saboury, I. Kostova, G. Benelli, F. Falahati, Green fabricated gold nanoparticles: synthesis, characterization, degradation of 4-nitrophenol from industrial wastewater, and insecticidal activity – a review, J. Clean. Prod. 184 (2018) 740–753.
[47] S.C.G. Kiruba Daniel, R. Kumar, V. Sathish, M. Sivakumar, S. Sunitha, T. Anitha, Sironmani, Green synthesis (*Ocimum tenuiflorum*) of silver nanoparticles and toxicity studies in zebra fish (*Danio rerio*) model, J. Nanosci. Nanotechnol. 2 (2011) 103–117.
[48] G. Benelli, F. Maggi, R. Pavela, K. Murugan, M. Govindarajan, B. Vaseeharan, R. Petrelli, L. Cappellacci, S. Kumar, A. Hofer, M.R. Youssefi, Abdullah A. Alarfaj, J.S. Hwang, A. Higuchi, Mosquito control with green nanopesticides: towards the one Health approach? A review of non-target effects, Environ, Sci. Pollut. Res. Int. (2018), https://doi.org/10.1007/s11356-017-9752-4.
[49] Q. Li, V. Wing-Wah Yam, High-yield synthesis of selenium nanowires in water at room temperature, Chem. Commun. (2006) 1006–1008.
[50] S. Vijayakumar, B. Vaseeharan, B. Malaikozhundan, M. Shobiya, *Laurus nobilis* leaf

extract mediated green synthesis of ZnO nanoparticles: characterization and biomedical applications, Biomed. Pharmacother. 84 (2016) 1213–1222.
[51] A. Thirunarayanan, S. Raja, G. Mohanraj, P. Rajakumar, Synthesis of chiral core based triazole dendrimers with m-terphenyl surface unit and their antibacterial studies, RSC Adv. 4 (2014) 41778–41783.
[52] M. Divya, B. Vaseeharan, M. Abinanya, S. Vijayakumar, M. Govindarajan, N.S. Alharbi, S. Kadaikunnan, J.M. Khaled, G. Benelli, Biopolymer gelatin-coated zinc oxide nanoparticles showed high antibacterial, antibiofilm and anti-angiogenic activity, J. Photochem. Photobiol. B 178 (2017) 211–218.
[53] P. Stiefel, S.S. Emrich, K.M. Weber, Q. Ren, Critical aspects of using bacterial cell viability assays with the fluorophores SYTO® 9 and propidium iodide, BMC Microbiol. 36 (2015) 1–9.
[54] M. Abinaya, B. Vaseeharan, M. Divya, A. Sharmili, M. Govindarajan, N.S. Alharbi, S. Kadaikunnan, J.M. Khaled, G. Benelli, Bacterial exopolysaccharide (EPS)-coated ZnO nanoparticles showed high antibiofilm activity and larvicidal toxicity against malaria and Zika virus vectors, J. Trace Elem. Med. Biol. 45 (2018) 93–103.
[55] D. Das, B. Chandra Nath, P. Phukon, A. kalita, S.K. Dolui, Synthesis of ZnO nanoparticles and evaluation of antioxidant and cytotoxic activity, Colloids Surf. B Biointerfaces 111 (2013) 556–560.
[56] WHO, CTD/WHOPES/IC/96.1, Report of the WHO Informal Consultation on the Evaluation on the Testing of Insecticides 96 (1996), pp. 1–69.
[57] R. Song, Y. Feng, D. Wang, Z. Xu, Z. Li, X. Shao, Phytoalexin phenalenone derivatives inactivate mosquito larvae and root-knot nematode as Type-II photosensitizer, Sci. Rep. 7 (2017) 42058.
[58] M. Kieliszek, S. Błażejak, A. Bzducha-Wróbel, A. Kurcz, Effects of selenium on morphological changes in *Candida utilis* ATCC 9950 yeast cells, Biol. Trace Elem. Res. 169 (2016) 387–393.
[59] M. Kieliszek, S. Błażejak, M. Płaczek, Spectrophotometric evaluation of selenium binding by *Saccharomyces cerevisiae* ATCC MYA-2200 and *Candida utilis* ATCC 9950 yeast, J. Trace Elem. Med. Biol. 35 (2016) 90–96.
[60] M. Kieliszek, S. Błażejak, A. Bzducha-Wróbel, A.M. Kot, Effect of selenium on lipid and amino acid metabolism in yeast cells, Biol. Trace Elem. Res. (2018) 1–12, https://doi.org/10.1007/s12011-018-1390-2.
[61] N.P. Moller, K.E. Scholz-Ahrens, N. Roos, J. Schrezenmeir, Bioactive peptides and proteins from foods: indication for health effects, Eur. J. Nutr. 47 (2008) 171–182.
[62] J.E. Bandow, N. Metzler-Nolte, New ways of killing the beast: prospects for inorganic–organic hybrid nanomaterials as antibacterial agents, Chem. Bio. Chem. 10 (2009) 2847–2850.
[63] S. Jayanthi, R. Iswarya, S. Karthikeyan, B. Vaseeharan, Purification, characterization and functional analysis of the immune molecule lectin from the haemolymph of blue swimmer crab *Portunus pelagicus* and their antibiofilm properties, Fish Shellfish Immunol. 62 (2017) 227–237.
[64] S. Jayanthi, S. Shanthi, B. Vaseeharan, N. Gopi, M. Govindarajan, N.S. Alharbi, S. Kadaikunnan, J.M. Khaled, G. Benelli, Growth inhibition and antibiofilm potential of Ag nanoparticles coated with lectin, an invertebrate immune molecule, J. Photochem. Photobiol. B 170 (2017) 208–216.
[65] S. Lee, C. Kwon, B. Park, S. Jung, Synthesis of selenium nanowires morphologically directed by shinorhizobial oligosaccharides, Carbohydr. Res. 344 (2009) 1230–1234.
[66] R. Avendano, N. Chaves, P. Fuentes, E. Sánchez, J.I. Jiménez, M. Chavarría, Production of selenium nanoparticles in *Pseudomonas putida* KT2440, Sci. Rep. 6 (2016) 1–9, https://doi.org/10.1038/srep37155.
[67] M. Kieliszek, S. Błażejak, I. Gientka, A. Bzducha-Wróbel, Accumulation and metabolism of selenium by yeast cells, Appl. Microbiol. Biotechnol. 99 (2015) 5373–5382.
[68] X. Huang, X. Chen, Q. Chen, Q. Yu, D. Sun, J. Liu, Investigation of functional selenium nanoparticles as potent antimicrobial agents against superbugs, Acta Biomater. 30 (2016) 397–407.
[69] X. Gao, T. Gao, L. Zhang, Solution–solid growth of *a*-monoclinic selenium nanowires at room temperature, J. Mater. Chem. 13 (2003) 6–8.
[70] C.P. Shah, C. Dwivedi, K.K. Singh, M. Kumar, P.N. Bajaj, Riley oxidation: a forgotten name reaction for synthesis of selenium nanoparticles, Mater. Res. Bull. 45 (2010) 1213–1217.
[71] R. Rekha, B. Vaseeharan, R. Ishwarya, M. Anjugam, N.S. Alharbi, S. Kadaikunnan, J.M. Khaled, M.N. Al-anbr, M. Govindarajan, Searching for crab-borne antimicrobial peptides: crustin from *Portunus pelagicus* triggers biofilm inhibition and immune responses of *Artemia salina* against GFP tagged *Vibrio parahaemolyticus* Dahv2, Mol. Immunol. 101 (2018) 396–408.
[72] P. Huang, L. Bao, D. Yang, G. Gao, J. Lin, Z. Li, C. Zhang, D. Cui, Protein-directed solution-phase green synthesis of BSA-conjugated M_xSe_y(M = Ag, Cd, Pb, Cu) Nanomaterials, Chem. Asian J. 6 (2011) 1156–1162.
[73] Y. Li, J.J. Zhang, J. Xuan, L.P. Jiang, J.J. Zhu, Fabrication of a novel nonenzymatic hydrogen peroxide sensor based on Se/Pt nanocomposites, Electrochem. commun. 12 (2010) 777–780.
[74] A. Ali, Won-Chun Oh, Preparation of nanowire like WSe2-Graphene nanocomposite for photocatalytic reduction of CO_2 into CH_3OH with the presence of sacrificial agents, Sci. Rep. 7 (2017) 1–11.
[75] T. Uhlig, T. Kyprianou, F.G. Martinelli, C.A. Oppici, D. Heiligers, D. Hills, X.R. Calvo, P. Verhaert, The emergence of peptides in the pharmaceutical business: from exploration to exploitation, EuPA Open Proteom. 4 (2014) 58–69.
[76] L. Liu, C. He, J. Li, J. Guo, D. Yang, J. Wei, Green synthesis of silver nanowires via ultraviolet irradiation catalyzed by phosphomolybdic acid and their antibacterial properties, New J. Chem. 37 (2013) 2179.
[77] F. Al-Hazmi, F. Alnowaiser, A.A. Al-Ghamdi, Attieh A. Al-Ghamdi, M.M. Aly, R.M. Al-Tuwirqi, F. El-Tantawy, A new large–scale synthesis of magnesium oxide nanowires: structural and antibacterial properties, Superlattices Microstruct. 52 (2012) 200–209.
[78] P.A. Tran, T.J. Webster, Selenium nanoparticles inhibit *Staphylococcus aureus* growth, Int. J. Nanomedicine 6 (2011) 1553–1558.
[79] S. Hou, H. Zhao, L. Zhao, Q. Shen, K.S. Wei, D.Y. Suh, A. Nakao, M.A. Garcia, M. Song, T. Lee, B. Xiong, S.C. Luo, H.R. Tseng, H. Yu, Capture and stimulated release of circulating tumor cells on polymer-grafted silicon nanostructures, Adv. Mater. 25 (2013) 1547–1551.
[80] Q. Shen, L. Xu, L. Zhao, D. Wu, Y. Fan, Y. Zhou, W.H. Ouyang, X. Xu, Z. Zhang, M. Song, T. Lee, M.A. Garcia, B. Xiong, S. Hou, H.R. Tseng, X. Fang, Specific capture and release of circulating tumor cells using aptamer-modified nanosubstrates, Adv. Mater. 25 (2013) 2368–2373.
[81] W.Y. Hong, S.H. Jeon, E.S. Lee, Y. Cho, An integrated multifunctional platform based on biotin-doped conducting polymer nanowires for cell capture, release, and electrochemical sensing, Biomaterials 35 (2014) 9573–9580.
[82] L. Liu, S. Chen, Z. Xue, Z. Zhang, X. Qiao, Z. Nie, D. Han, J. Wang, T. Wang, Bacterial capture efficiency in fluid bloodstream improved by bendable nanowires, Nat. Commun. 444 (2018) 1–9.
[83] X. Liu, L. Chen, H. Liu, G. Yang, P. Zhang, D. Han, S. Wang, L. Jiang, Bio-inspired soft polystyrene nanotube substrate for rapid and highly efficient breast cancer-cell capture, NPG Asia Mater. 5 (2013) e63.
[84] Y.Q. Li, B. Zhu, Y. Li, W.R. Leow, R. Goh, B. Ma, E. Fong, M. Tang, X. Chen, A synergistic capture strategy for enhanced detection and elimination of bacteria, Angew. Chem. Int. Ed. 53 (2014) 5837–5841.
[85] M. Divya, B. Vaseeharan, M. Anjugam, A. Iswarya, S. Karthikeyan, P. Velusamy, M. Govindarajan, N.S. Alharbi, S. Kadaikunnan, J.M. Khaled, C. Vagvolgyi, Phenoloxidase activation, antimicrobial, and antibiofilm properties of β-glucan binding protein from *Scylla serrata* crab hemolymph, Int. J. Biol. Macromol. 114 (2018) 864–873.
[86] S. Ramya, T. Shanmugasundaram, R. Balagurunathan, Biomedical potential of actinobacterially synthesised selenium nanoparticles with special reference to antibiofilm, anti-oxidant, wound healing, cytotoxic and anti-viral activities, J. Trace Elem. Med. Biol. 32 (2015) 30–39.
[87] G. Benelli, Plant-mediated biosynthesis of nanoparticles as an emerging tool against mosquitoes of medical and veterinary importance: a review, Parasitol. Res. 115 (2016) 23–34.
[88] G. Benelli, Green synthesized nanoparticles in the fight against mosquito-borne diseases and cancer −a brief review, Enzyme Microb. Technol. 95 (2016) 58–68.
[89] M. Govindarajan, M. Rajeswary, U. Muthukumaran, S.L. Hoti, H.F. Khater, G. Benelli, Single-step biosynthesis and characterization of silver nanoparticles using *Zornia diphylla*leaves: A potent eco-friendly tool against malaria and arbovirus vectors, J. Photochem. Photobiol. B 161 (2016) 482–489.
[90] K. Murugan, V. Priyanka, D. Dinesh, P. Madhiyazhagan, C. Panneerselvam, J. Subramaniam, U. Suresh, B. Chandramohan, M. Roni, M. Nicoletti, A.A. Alarfaj, A. Higuchi, M.A. Munusamy, H.F. Khater, R.H. Messing, G. Benelli, Predation by Asian bullfrog tadpoles, *Hoplobatrachus tigerinus*, against the dengue vector, *Aedes aegypti*, in an aquatic environment treated with mosquitocidal nanoparticles, Parasitol. Res. 114 (2015) 3601–3610.
[91] R. Ishwarya, B. Vaseeharan, R. Anuradha, R. Rekha, M. Govindarajan, N.S. Alharbi, S. Kadaikunnan, Jamal M. Khaled, G. Benelli, Eco-friendly fabrication of Ag nanostructures using the seed extract of *Pedalium murex*, an ancient Indian medicinal plant: histopathological effects on the Zika virus vector *Aedes aegypti* and inhibition of biofilm-forming pathogenic bacteria, J. Photochem. Photobiol. B 174 (2017) 133–143.
[92] M. Saxena, S.K. Sonkar, S. Sarkar, Water soluble nano carbons arrest the growth of mosquito, RSC Adv. 12 (2013) 1–6.
[93] G. Volohonsky, A.-K. Hopp, M. Saenger, J. Soichot, H. Scholze, J. Boch, S.A. Blandin, E. Marois, Transgenic expression of the anti-parasitic factor TEP1 in the malaria mosquito *Anopheles Gambiae*, PLoS Pathog. 13 (2007) e1006113.
[94] A.M. Fallon, Flow cytometric evaluation of the intracellular bacterium, *Wolbachia pipientis*, in mosquito cells, J. Microbiol. Methods 107 (2014) 119–125.